remote sensing

MDPI

Article

Characterization of Active Riverbed Spatiotemporal Dynamics through the Definition of a Framework for Remote Sensing Procedures

Marta Crivellaro [1], Alfonso Vitti [2,*], Guido Zolezzi [1,2] and Walter Bertoldi [1,2]

[1] Center Agriculture Food Environment, University of Trento, 38098 San Michele all'Adige, Italy; marta.crivellaro@unitn.it (M.C.); guido.zolezzi@unitn.it (G.Z.); walter.bertoldi@unitn.it (W.B.)
[2] Department of Civil, Environmental and Mechanical Engineering, University of Trento, 38123 Trento, Italy
* Correspondence: alfonso.vitti@unitn.it

Abstract: The increasing availability and quality of remote sensing data are changing the methods used in fluvial geomorphology applications, allowing the observation of hydro-morpho-biodynamics processes and their spatial and temporal variations at broader and more refined scales. With the advent of cloud-based computing, it is nowadays possible to reduce data processing time and increase code sharing, facilitating the development of reproducible analyses at regional and global scales. The consolidation of Earth Observation mission data into a single repository such as Google Earth Engine (GEE) offers the opportunity to standardize various methods found in literature, in particular those related to the identification of key geomorphological parameters. This work investigates different computational techniques and timeframes (e.g., seasonal, annual) for the automatic detection of the active river channel and its multi-temporal aggregation, proposing a rational integration of remote sensing tools into river monitoring and management. In particular, we propose a quantitative analysis of different approaches to obtain a synthetic representative image of river corridors, where each pixel is computed as a percentile of the bands (or a combination of bands) of all available images in a given time span. Synthetic images have the advantage of limiting the variability of individual images, thus providing more robust results in terms of the classification of the main components of the riverine ecosystem (sediments, water, and riparian vegetation). We apply the analysis to a set of rivers with analogous bioclimatic conditions and different levels of anthropic pressure, using a combination of Landsat and Sentinel-2 data. The results show that synthetic images derived from multispectral indexes (such as NDVI and MDWI) are more accurate than synthetic images derived from single bands. In addition, different temporal reduction statistics affect the detection of the active channel, and we suggest using the 90th percentile instead of the median to improve the detection of vegetated areas. Individual representative images are then aggregated into multitemporal maps to define a systematic and easily replicable approach for extracting active river corridors and their inherent spatial and temporal dynamics. Finally, the proposed procedure has the potential to be easily implemented and automated as a tool to provide relevant data to river managers.

Keywords: remote sensing; active channel; riverine macro units; synthetic representative images; Google Earth Engine

Citation: Crivellaro, M.; Vitti, A.; Zolezzi, G.; Bertoldi, W. Characterization of Active Riverbed Spatiotemporal Dynamics through the Definition of a Framework for Remote Sensing Procedures. *Remote Sens.* **2024**, *16*, 184. https://doi.org/10.3390/rs16010184

Academic Editors: Michael Nones, Maria Nicolina Papa and Paolo Paron

Received: 17 October 2023
Revised: 23 December 2023
Accepted: 27 December 2023
Published: 1 January 2024

1. Introduction

Remote sensing (RS) plays a crucial role in advancing the scientific understanding and monitoring of riverscapes [1–4]. This is converting river science from a data-poor to a data-rich discipline [5], transforming the methods employed in fluvial observation, and boosting integrative approaches. Technical advances in RS have already enabled the observation of spatial and temporal changes at larger and more precise scales, with the ability to replicate findings at local, regional, and global scales using a non-intrusive approach. Moreover, RS has enhanced the interdisciplinarity of river science by building

bridges among studies of hydrology, ecosystem functionality, restoration, and geomorphic evolution. In terms of the improved understanding of riverine processes, RS has contributed to the comprehension of mass and energy transfer through riverscapes [6], the extraction of water surfaces, the observation of their variation throughout time [7], and the recognition of the role of sediment and vegetation in channel conveyance [8]. RS has also enabled the baseline assessment of fluvial morphology in data-fragmented contexts [8,9] and the outlining of hydrological variations, such as in Arctic regions [10]. As a tool for river management and conservation, RS is widely recognized for its ability to reconstruct recent morphological trajectories [11–14] and to assess morphological condition [15,16]. Satellite data combined with hydrological measurements can also support the monitoring of river restoration works at the reach scale [17]. The advent of cloud-based computing has further revolutionized the field by providing access to publicly available global remote sensing datasets (USGS NASA Landsat and ESA Sentinel products, among others) in a unified environment, resulting in accelerated data processing and improved code portability [18]. Platforms such as Google Earth Engine have been instrumental in various river-related studies, including mapping wet river channels [19], assessing the frequency and extent of water occurrence [7], identifying active channels [8,20], estimating river width [21], and monitoring the migration of active channels near critical infrastructure [14].

Traditional remote sensing GIS-based analyses are well-established tools to support river research and management [22], with coherent use of different remote sensing tools to investigate processes at different spatiotemporal scales [23]. With the advent of cloud computing, there is a need for appropriate methods to organize and aggregate remote sensing data. In fact, cloud-based semi-automated or automated analysis is still in its infancy in its interdisciplinary framework, and basic reference work is needed to define which data aggregation procedures can and should be used at different spatiotemporal scales, according to the fluvial morphodynamic or ecological process to be observed.

We focus here on the possibility given by GEE to work with synthetic representative images, where all images acquired in a defined temporal interval are reduced together to obtain a more robust synthetic representative image. From the obtained representative image, we propose an approach to extract a specific element of any riverscape, the active or erodible corridor [24], which we identify as the multitemporal active channel. In 2013, Ashmore described active channels as *"those transporting bedload or showing measurable morphological change at a given time or during a given time interval"* [25]. This definition highlights the need to contextualize not only the river system we consider in space and time but also the lenses we use to observe morphological change. Thus, we consider an active channel as part of a river landscape that experiences measurable morphological planform changes through medium-resolution remote sensing imagery. Using this definition, we aim to explore the capabilities and limitations of the Google Earth Engine (GEE) cloud computing platform in supporting the detection of total active channel area and how it changes over different temporal scales.

First, we focus on different ways to define a synthetic image of a river corridor. Synthetic images reduce the inherent variability of individual images, resulting in more robust results for classifying key components of river ecosystems, or macro units (see [26], such as the sediment bar, water, and riparian vegetation). Although this is an accepted common approach to obtain a representative observation of the environmental system [8,27], to the best of our knowledge, no consideration has been given to how to obtain such an image taking into account the spatiotemporal scales of changes in river morphology, where for certain processes it is key to study the effects of this variability rather than smoothing it. In GEE, we calculate each pixel of a synthetic image as a percentile of the distribution of the same pixel values within a specified time interval. We outline how different percentiles impact synthetic images and, consequently, the automatic detection of active channels using Landsat and Sentinel-2 products. With the aim of defining a systematic approach, our work clarifies appropriate statistics and timeframes (e.g., seasonal, annual) for calculating representative images based on research objectives.

Thus, this research explicitly frames existing technologies within the nested spatiotemporal scale of fluvial biogeomorphic processes and improves a more conscious integration of remote sensing tools into river monitoring and management. Finally, this work opens the box of spatiotemporal metrics for river assessment: a multitemporal active channel is proposed as the envelope of active channels in each year of observation, shifting from single epoch metrics to inter-epoch ones. Such a procedure supports the extraction of the fluvial erodible corridor, which represents a piece of reference information for river managers, with an improved standardized approach that considers and brings to light the inherent dynamicity of riverscapes in space and time, including the spatially explicit relative frequency of the river occupying its space of freedom.

2. Materials and Methods

In this work, Google Earth Engine is used to extract information on the riverine active channel extension from multi-spectral medium-resolution satellite imagery, namely Landsat and Sentinel-2 surface reflectance products. The selected study areas for the methodological work are three river reaches in the Mediterranean region with analogous bioclimatic conditions and different degrees of anthropic pressure, to obtain more robust and representative results for the considered cases.

2.1. Google Earth Engine Workflow

Landsat Surface Reflectance data (Landsat 5 Thematic Mapper, Landsat 7 Enhanced Thematic Mapper, Landsat 8 Operational Land Imager) and Harmonized Sentinel-2 MSI: MultiSpectral Instrument, Level-2A, are selected as the primary sources of satellite imagery (available through the GEE data catalog https://developers.google.com/earth-engine/datasets/catalog, accessed on 15 April 2023). Landsat products are widely used to assess recent spatiotemporal morphological changes [8,14,28], thanks to their almost continuous coverage of satellite images within the analysis period (1985–2022) and a spatial resolution of 30 m. Similarly, since 2015, Sentinel-2 images provide higher spatial (10 m) and temporal resolution multispectral information worldwide (the revisit time is 10 days at the equator with 1 satellite and 5 days with two satellites under cloud-free conditions). Sentinel-2 Level-2A orthorectified atmospherically corrected surface reflectance products have been available in GEE since 2017.

Images with cloud cover greater than 20% were excluded from Landsat and Sentinel-2 collections. A spatial clip was applied to the selected images, limiting the region of interest on each river reach. Moreover, the CFmask algorithm [29], which is based on pixel quality assessment, is applied to each Landsat image in the collection to mask cloud obstructions and cloud shadows. An analogous cloud mask is applied to Sentinel-2 images by filtering clouds and cirrus directly from the image metadata information. The two temporal synthetic resolutions compared in this work are the Seasonal—covering the vegetative season (May to September)—and the annual (January to December), for each year of the considered temporal extent, set from 1985 to 2022, with Sentinel-2 images available from 2018 (Figure 1).

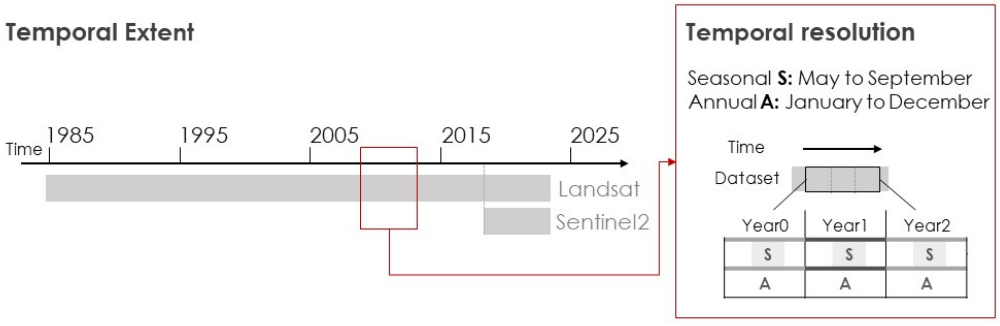

Figure 1. Temporal extent and resolution of the analysis.

The workflow is subdivided into three parts:

1. Identification of the most appropriate procedure to derive a synthetic representative image for a given synthetic temporal resolution.
2. Extraction of the representative active channel for a given synthetic temporal resolution.
3. Computation of the multitemporal active channel as the envelope of all extracted active channels over time for the entire temporal extent of the analysis.

2.1.1. Representative Synthetic Index

In GEE, Landsat and Sentinel-2 images are structured as an *ImageCollection*, a stack, or a time series of images. For an *ImageCollection*, it is possible to apply a *Reducer*, which can be used to aggregate data over time, space, and other data structures. *Reducers* include summary statistics, histograms, and linear regression, among others. Thus, it is possible to obtain *ImageCollection* statistics over time and obtain a representative synthetic image, with reduction operations occurring on a pixel-by-pixel basis. When working with multispectral images in riverscapes, several multi-spectral indexes and combinations support highly differentiated fluvial geomorphology applications [9,11]. In this work, we selected two established multi-spectral indexes to map vegetated surfaces and water, to derive active channel extension, namely the Normalized Difference Vegetation Index, NDVI [30], and the Modified Normalized Water Index, MNDWI [31].

A common approach to mapping riverine macro units is based first on the use of GEE temporal reduction (Figure 2 Panel 1) on image bands and then on the computation of multi-spectral indexes from the reduced maps [28,32] (Figure 2 Panel 2, procedure 2A). Here, we propose a different approach where NDVI and MNDWI multispectral indexes are firstly computed for each image of the *ImageCollection* (Landsat and Sentinel-2). Secondly, the temporal reduction is applied to the collection of indexes (Figure 2 Panel 2, procedure 2B). To evaluate the synthetic indexes derived with the two approaches—*(i)* reduced bands and *(ii)* reduced indexes at the annual temporal resolution—and the macro units that can be derived consequently, we considered a reference active channel of one of the selected river reaches, digitized in QGIS from the 2015 Orthophoto with 20 cm resolution, available as WMS from the Albanian geoportal ASIG services [33]. Moreover, the reference active channel was extracted with a buffer of 200 m to properly assess the medium-resolution Landsat accuracy with the semi-automatic extraction at the borders of the river corridor.

2.1.2. Representative Active Channel

The second step of our workflow goes through the delineation of the active channel for the considered temporal resolutions. GEE offers the possibility to use several spatial and temporal statistical reducers. So far, the temporal median reducer, which gives each pixel its median value over the considered time step, has been used to extract fluvial morphological metrics [28,32]. A comparison between the median (50p) and the 90th percentile (90p) reducer is proposed here. To do so, we classify potential active channels in every pixel with a 50p or 90p synthetic representative NDVI lower than 0.15 [32] and an MNDWI greater than -0.35, similarly to [8]. Thus, the potential active channel area is evaluated by comparing 50p and 90p, seasonal and annual extracted masks. In this step, areas mapped as active channels but clearly external to the riverscape are retained to compare how well 50p, 90p, seasonal and annual choices are able to distinguish riverscapes from other external areas and to compare our approach with other existing ones.

2.1.3. Multitemporal Active Channel

The third and final step in our workflow is the delineation of the envelope of all previously detected seasonal or annual active channels. The envelope represents the multitemporal active channel domain or the so-called erodible corridor. It results from the spatial evolution in time of the riverine active channel. It can be extracted as the envelope of individual representative active channels, where the value of each pixel is the number of times it is classified as the active channel divided by the considered temporal extent. This

produces a final map ranging from 0 to 1. Pixels are included in the multitemporal active channel when they are active for at least a fixed threshold, excluding low-frequency pixels.

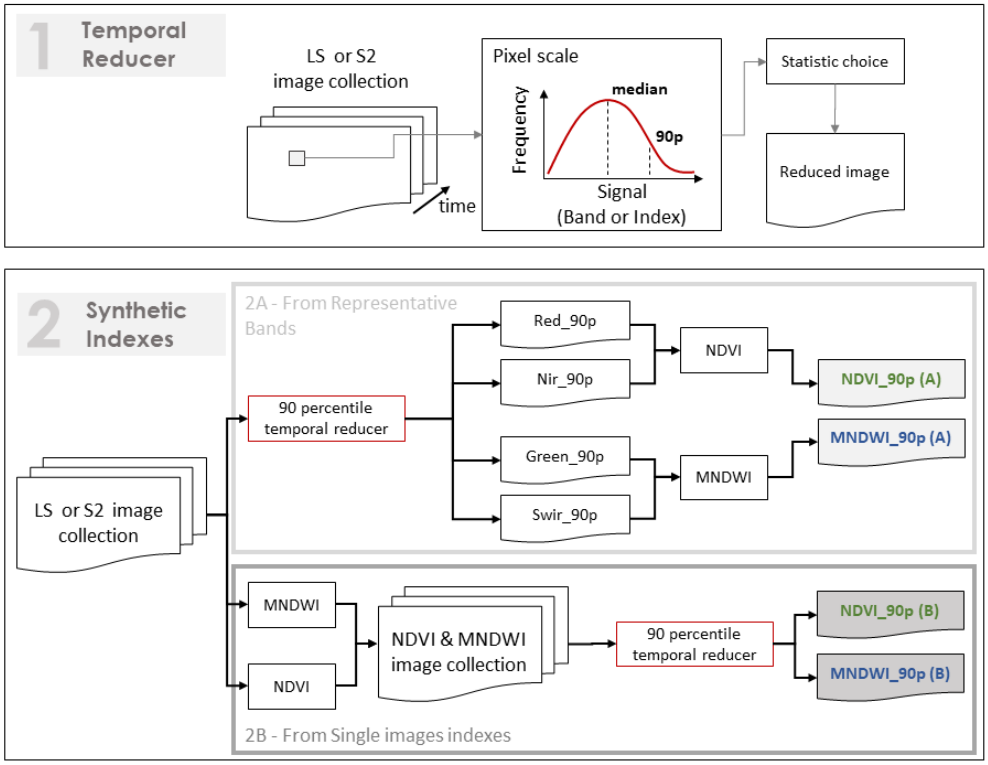

Figure 2. Workflow to obtain synthetic representative images of NDVI and MNDWI composites and to assess their difference. Panel 1: Temporal reducer over an ImageCollection. Panel 2: Synthetic images approaches compares: Panel 2A showsthe traditional approach of representative bands and Panel 2B outlinesthe proposed novel approach that reduces single images multispectral indexes.

In this work we have used a threshold of 27% (10 counted times in the temporal extent 1985–2022), but we suggest to define it according to each study objective. We computed four different envelopes considering (i) the 50p and 90p of the indexes and (ii) seasonal or annual synthetic temporal resolution. Envelopes were computed for the period 1985 to 2022 using Landsat images, and for the overlapping period 2018–2022 using both Landsat and Sentinel-2 images.

2.2. Study Areas

The procedure is applied at the river reach scale to a set of three case studies (Figure 3): the Shkumbin (AL), Tagliamento (IT), and Vjosa (AL) rivers. The Tagliamento and Vjosa rivers are recognized as reference fluvial systems and model ecosystems of European importance [34,35]. Conversely, the Shkumbin River received less attention. It flows through Albania and has been impacted by the abrupt socio-economical development of Albania in the last two decades; sediment mining activities within the active channel can be easily detected from aerial images of recent years [36].

River reaches were selected among river systems where active channel morphological changes and trajectories have already been investigated [9,37,38]. Selected reaches are much wider than the minimum size required to achieve sufficient accuracy with Landsat imagery. The river width should be at least 10 times the pixel spatial resolution to limit the error below 20% [39], setting 300 m and 100 m as width thresholds for Landsat and Sentinel-2 images, respectively. Moreover, all selected reaches present a braiding morphology (Table 1), which can be considered an optimal river style for testing active channel extraction procedures. In fact, in braided rivers at low flow the wet channel extracted by standard water-related

multispectral indexes covers only a small portion of the active channel spatiotemporal dynamics, with sediments and in-channel vegetation patches playing a relevant role in the hydro-morpho-eco dynamics of the riverscape.

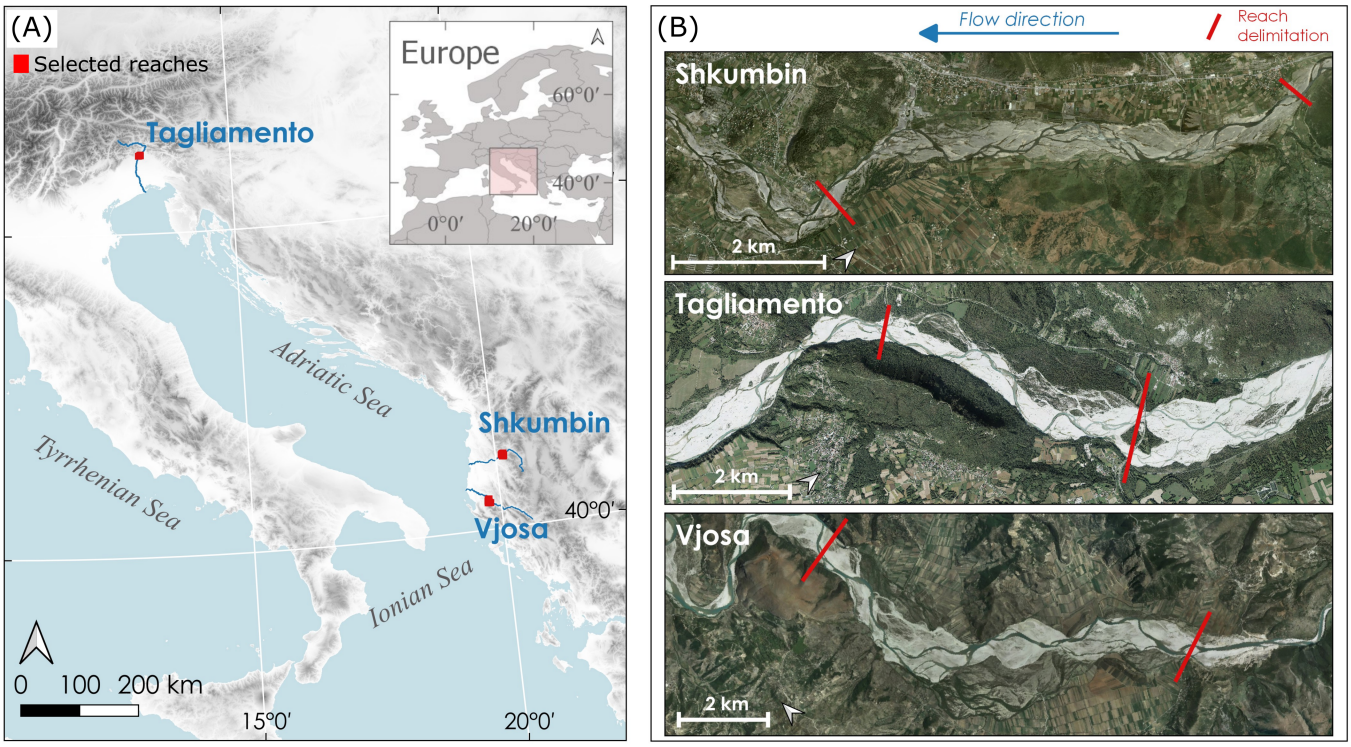

Figure 3. Panel (**A**): Location of the selected rivers; Panel (**B**): Selected river reaches overview. The basemap orthophoto for Shkumbin and Vjosa rivers is the 2015 ASIG Orthophoto [33], while the Tagliamento basemap is 2017–2020 Friuli Venezia Giulia regional Orthophoto [40].

Table 1. Key characteristics of selected river reaches.

Morphological Metric	Shkumbin	Tagliamento	Vjosa
Entire river length [km]	173	172	272
Catchment area [km^2]	2057	2580	6704
Contributing catchment area to the study reach [km^2]	604 (29%)	2300 (88%)	5242 (78%)
Reach confinement [1]	Partially Confined	Confined	Partially Confined
Reach morphology [1]	Braiding	Braiding	Braiding
Reach lenght [km]	6.9	4.8	6.9
Mean river corridor width [m]	500	600	800
Reach Slope [%]	0.45	0.36	0.18

[1] Following IDRAIM River Styles classification [41].

2.2.1. Shkumbin River

The Shkumbin River flows east-west in the central part of Albania to the Adriatic Sea. It is known for its relevant sediment load [42], comparable to the annual sediment load of the Vjosa river, which has a three times larger catchment area [43]. The selected reach is a partially confined 7 km-long reach in the Hill physiographic unit, flowing near the city of Elbasan. The reach has an average width of 450 m.

2.2.2. Tagliamento River

The Tagliamento River is located in the Friuli Venezia Giulia Region, northeastern Italy. The funnel-shaped catchment has an area of about 2580 km^2. Strong changes in flow

energy, sediment size, and distribution occur along the river's 170 km course. The climate is alpine in the headwaters and Mediterranean in the lower reaches, giving the river a flashy flow regime [44]. The selected reach presents an island-braided channel pattern, confined between Ragogna and Monte Prat, just upstream of the Pinzano bridge.

2.2.3. Vjosa River

The Vjosa river originates in the Pindos Mountains of Greece and flows for 272 km through southern Albania to the Adriatic Sea. The climate shifts from alpine in the headwaters to Mediterranean in the middle and lower reaches, giving the river a pluvio-nival regime. The selected Vjosa reach is a partially confined braided reach located in the middle course, in the Hill physiographic unit, near the village of Kuta. It presents a bar-braiding and island-braiding morphology, with an average width of 800 m. The reach flows in a medium-energy non-cohesive Holocene alluvial gravel-bed floodplain [45].

3. Results

3.1. Representative Synthetic Index

First, NDVI and MNDWI were investigated in the selected reaches, as well as the derived macro units (vegetation and water, respectively) in terms of value distributions and spatial configurations. Secondly, the active channel, defined as the union of water and sediment pixels, was extracted and compared between the traditional "bands" approach and the proposed "indexes" approach. Figure 4 shows the comparison between the two approaches. Panel A shows synthetic MNDWI and NDVI indexes derived from reduced bands and reduced indexes and compares their frequency histograms. The red line within the histogram represents the adopted fixed threshold for classifying water and non-water pixels (MNDWI) and vegetated and unvegetated pixels (NDVI). Within the extracted water and vegetation masks, Panel B shows the comparison between water and vegetation masks and the distribution of multispectral indexes values within the extracted masks. Representative synthetic image definition and the comparison between representative indexes derived from (i) synthetic bands or (ii) synthetic indexes outline relevant differences between the two approaches. The representative synthetic MNDWI and NDVI frequency distributions peak at lower values for the indexes approach (Figure 4, yellow) compared to the bands approach (Figure 4, light blue), with higher frequencies of high values of MNDWI (representing water). The NDVI frequency distribution obtained with the indexes approach (Figure 4, yellow) is wider than that derived with the bands approach (Figure 4, light blue).

A fixed threshold of MNDWI is set to quantitatively compare the two approaches. The threshold is set to 0.15, which is conservatively lower than the 0.2 value suggested for water detection by [46], to investigate the different MNDWI values in correspondence of water boundaries. The results show that the extent of water and vegetation is higher with the indexes approach (Figure 4, Panel b, yellow area). Moreover, all water and vegetation pixels detected with the synthetic bands (Figure 4, Panel b, light blue) are also masked with those detected by the indexes approach (yellow). As for the NDVI threshold, every pixel with an NDVI value higher than 0.15 is classified as vegetation [32,47]. Looking at the NDVI and MNDWI values within the masked water and vegetation pixels, it can be seen that the masks obtained from the indices have slightly higher values in their distributions. This difference is more pronounced for the MNDWI index (Figure 4, Panel b).

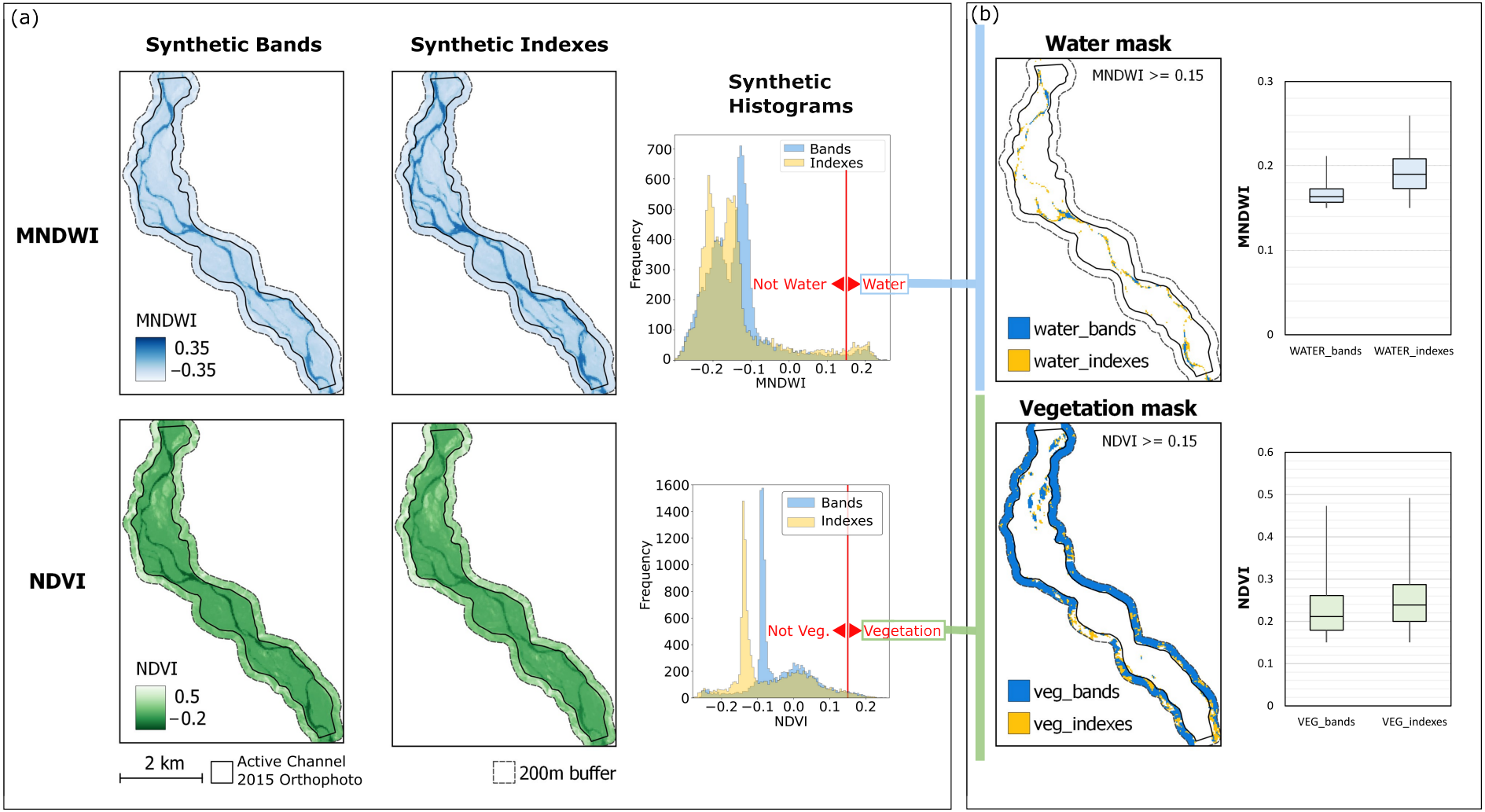

Figure 4. Comparison between bands and indexes approaches using representative synthetic index images (**a**) Synthetic MNDWI and NDVI indexes derived from reduced bands and reduced indexes and their histogram frequency. The red line within the histogram represents the adopted fixed threshold to classify water and non-water pixels (MNDWI) and vegetated and unvegetated pixels (NDVI). (**b**) Spatial water and vegetation masks derived from the two approaches, and distributions of MNDWI and NDVI values within the extracted masks.

Moreover, Figure 5 shows that the indexes approach identifies a more accurate extraction of the active channel (water and sediment areas) compared to that obtained with the bands approach. The difference Panel in Figure 5 highlights that the differences in the classification are mainly located in the lateral buffer and correspondence of riverine islands.

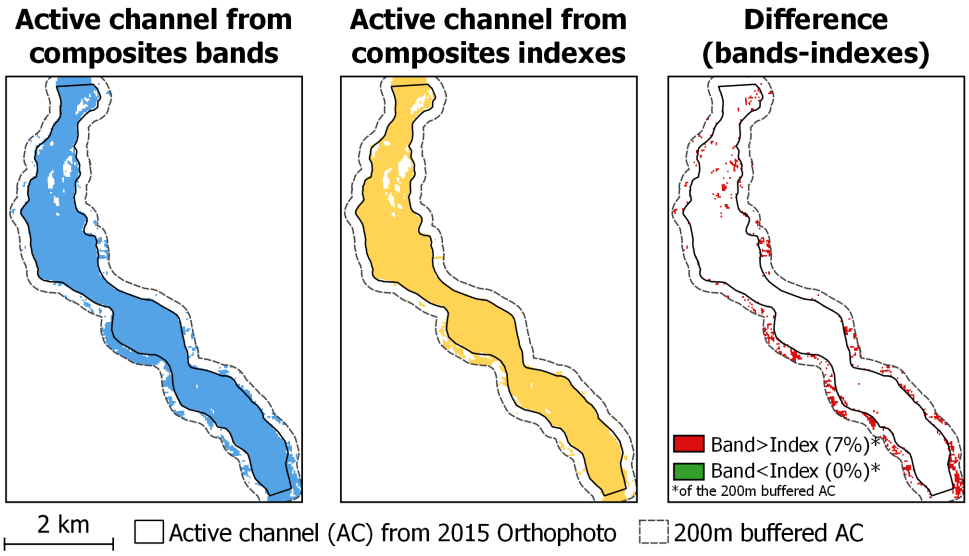

Figure 5. Active channel extracted with the bands approach (light blue) and with the indexes approach (yellow) compared to the digitized active channel from 2015 Orthophoto (continuous black line). The dotted line represents the 200 m buffered domain for the analysis. The difference map on the right outlines the difference between the two extracted active channels, showing the overestimation with the bands approach.

3.2. Representative Active Channel

Active channel extraction from the median and 90p NDVI synthetic images outlines the larger extent of the active channel obtained with the 50p image compared to the 90p image, for both seasonal and annual temporal extents in all three considered rivers (Figure 6). This difference appears to be influenced by the floodplain and riparian vegetation type, which are influenced by climate and land use.

The annual active channel appears to be substantially different from the seasonal active channel in the case of the 50p reduction choice, while smaller discrepancies can be seen using the 90p reducer. This is explained by the fact that the 50p NDVI values on the annual base are generally much lower than the seasonal ones, due to the winter dormancy of deciduous vegetation, which results in greater detection of active channel areas. This is less pronounced for the 90th percentile reduction option.

3.3. Multitemporal Active Channel

The third result of the workflow is the aggregation of active channels over time to obtain the multitemporal active channel. The comparison of different multitemporal active channels, obtained from different statistics and temporal resolutions, is proposed in terms of:

- Median and 90th percentile-derived multitemporal envelopes (Landsat, 1985–2022);
- Seasonal vs. annual 90th percentile-derived multitemporal envelopes (Landsat, 1985–2022);
- Coarser and finer spatial resolution–90th percentile-derived multitemporal envelopes (Landsat and Sentinel-2, 2018–2022).

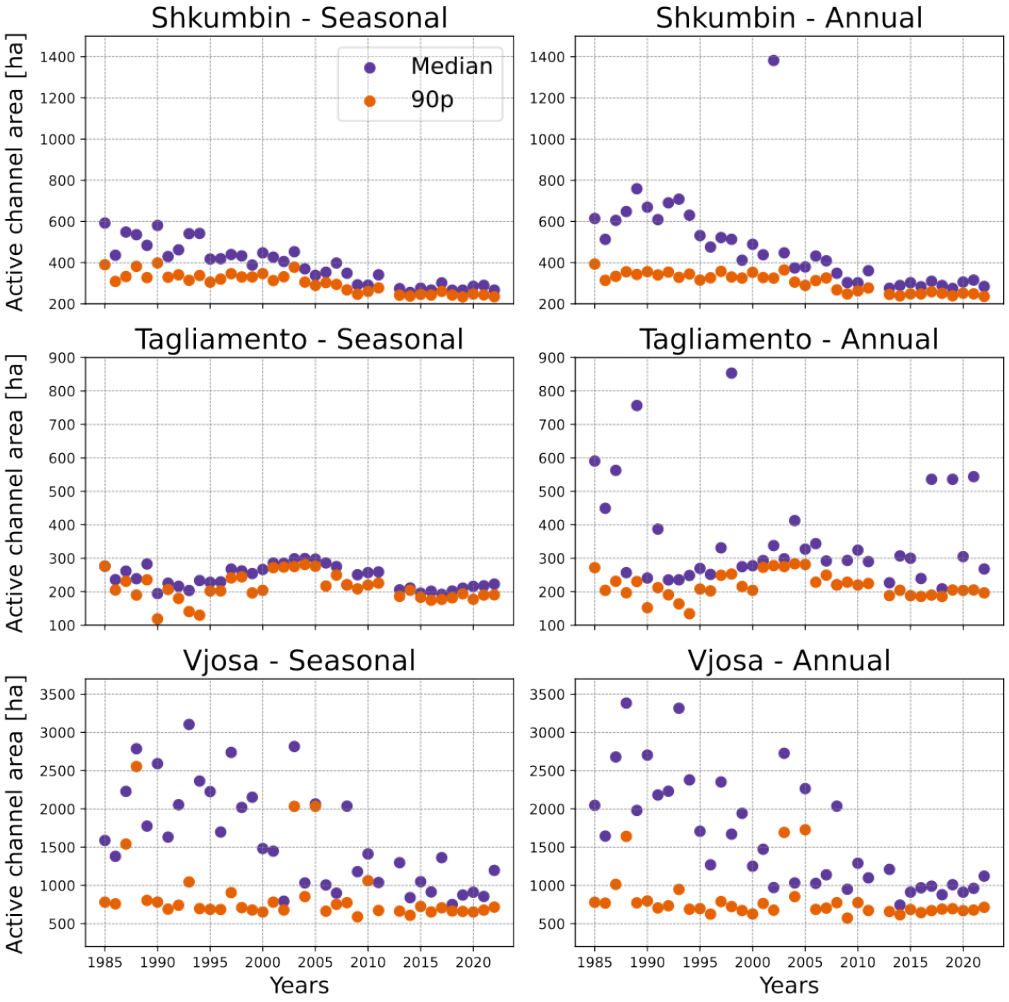

Figure 6. Seasonal and annual active channel extent per each year with 50p and 90p NDVI synthetic image classification.

3.3.1. Median and 90th Percentile-Derived Multitemporal Envelopes (Landsat, 1985–2022)

Comparing the median and 90th percentile-derived frequency envelopes (Figure 7), it is possible to outline the greater frequency of the median envelope with respect to the 90p envelope, as the difference between the two envelopes is never negative. This is particularly visible in the cultivated floodplain of the Vjosa river. Setting the defined threshold for multitemporal active channel detection to the envelope frequency, the filtered multitemporal active channel is obtained (Figure 7). It is easy to appreciate the improved noise removal of the 90p, which is able to exclude floodplain areas erroneously classified as multitemporal active channels when using the median (Table 2). This is particularly visible in the Shkumbin and Vjosa reaches, which are characterized by a cultivated floodplain, and less relevant in the Tagliamento reach, where the river reach is partially confined between forested slopes and floodplain.

Table 2. Multitemporal active channel area [ha]: Median and 90th percentile comparison, with frequency threshold t = 27%.

River	Median [ha]	90th Percentile [ha]	% Difference [1]
Shkumbin	471.7	384.0	22.8
Tagliamento	308.8	289.7	6.6
Vjosa	2183.1	871.4	150.5

[1] % difference is computed with respect to 90p mask.

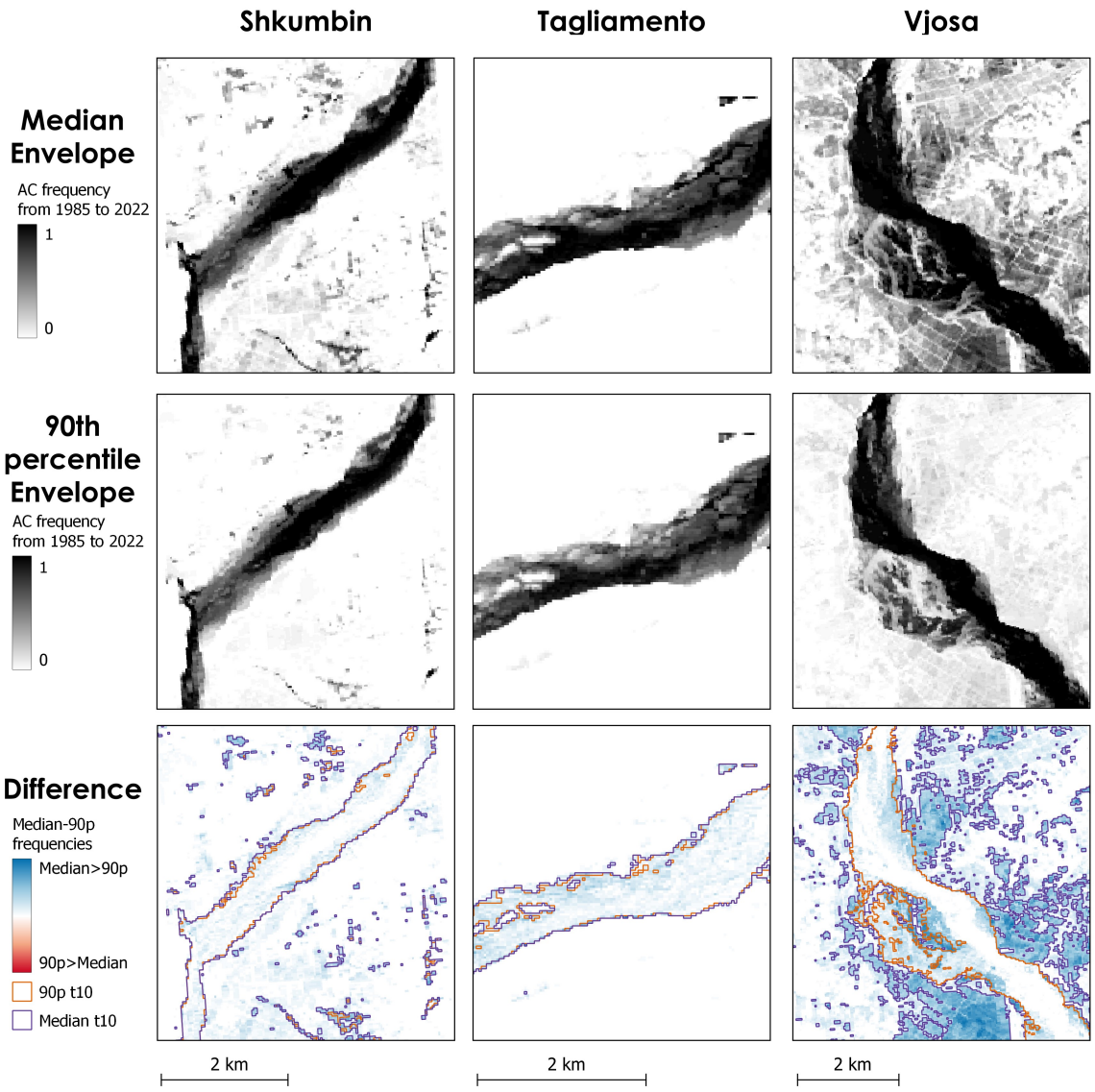

Figure 7. Landsat: Median and 90p active channel frequency envelopes, their difference and derived multitemporal active channel with a frequency threshold t = 27%.

3.3.2. Seasonal vs. Annual 90th Percentile-Derived Multitemporal Envelopes (Landsat, 1985–2022)

The annual-derived envelope includes all months in the active channel computation, while the Seasonal-derived envelope is restricted to the vegetative season (May to September in the selected case studies). They are compared in Figure 8 and Table 3 considering the region obtained by merging the 90th percentile annual envelope with a 300 m buffer to focus on the riverscape and its nearbies. Setting an appropriate threshold to define the multitemporal active channel from the frequency envelope (e.g., t = 27%) does not significantly change the multitemporal active channel area with respect to the annual envelope (1.5 to −1.3% difference, Table 3). Limited discrepancies in the active channel delineation can be detected in the lateral boundaries or in correspondence of vegetated islands and bars due to the different values between the Seasonal and Annual NDVI representative images (Figure 8). The difference between the Annual and Seasonal envelopes shows a higher frequency of the Annual envelope (difference > 0) within the active channel and higher frequencies of the Seasonal envelope (difference < 0) outside the active channel. This is especially noticeable for the Shkumbin and Vjosa floodplains, in correspondence

with cultivated areas, while it is less visible for the Tagliamento River, where the difference is almost nonexistent. This can be explained by the different land use (more forested parts along the river and less agricultural areas) and climate (more continental and less Mediterranean) of the Tagliamento with respect to the two Albanian rivers.

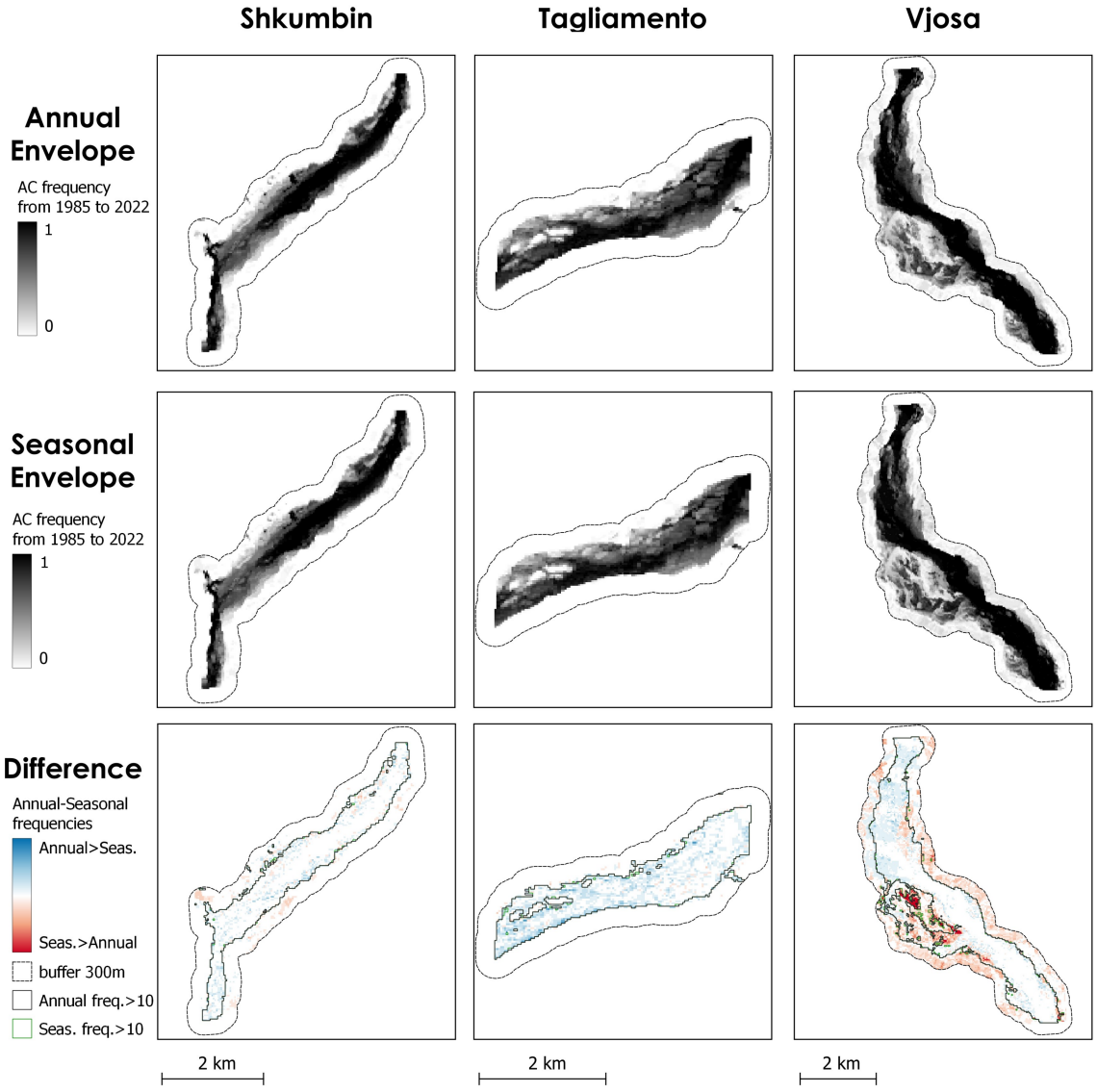

Figure 8. Annual and seasonal active channel envelopes derived from Landsat images.

Table 3. Multitemporal active channel area [ha]: annual and seasonal comparison, with selected frequency threshold t = 27%.

River	Annual [ha]	Seasonal [ha]	% Difference [1]
Shkumbin	384.0	378.6	1.4
Tagliamento	289.7	285.3	1.5
Vjosa	871.4	882.8	−1.3

[1] % difference is computed with respect to annual mask.

3.3.3. Comparing the Spatial Resolution of 90th Percentile-Derived Multitemporal Envelopes (Landsat and Sentinel-2, 2018–2022)

The spatial resolution comparison between 30 m Landsat and 10 m Sentinel images is coherent with the expected spatial smoothing of NDVI values representing vegetation in

Landsat images, with a consequent higher active channel frequency. This occurs especially in the boundary areas, as can be seen in Figure 9.

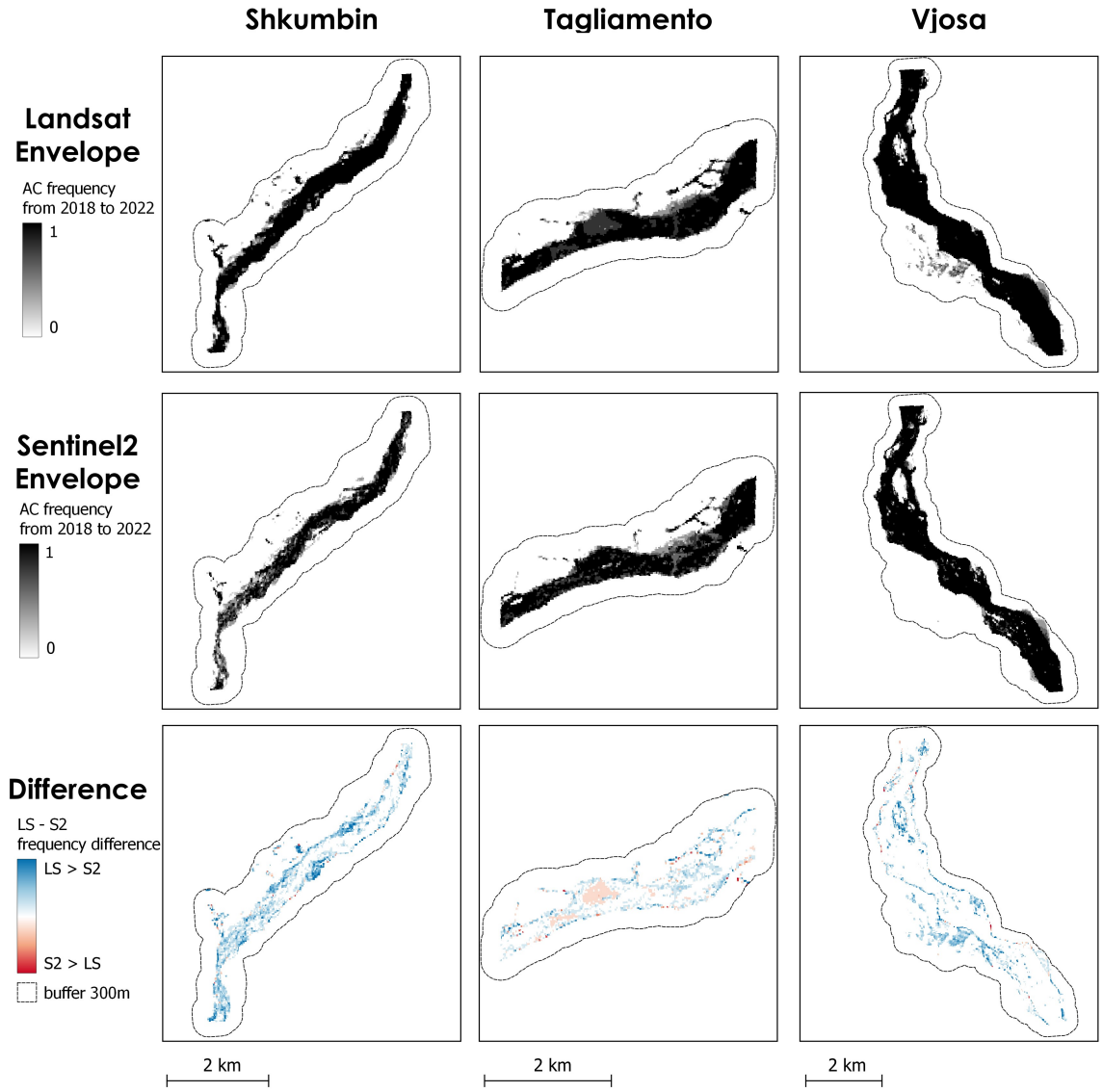

Figure 9. 2018–2022 annual active channel envelopes derived from Landsat and Sentinel-2 images.

4. Discussion

The availability of archives containing data from a variety of Earth observation missions, all consolidated in a unified database such as Google Earth Engine (GEE), combined with the ability to efficiently and consistently process this vast amount of data and information, underscores the need for a systematic approach. This provides an opportunity to standardize the diverse methodologies advocated in the existing literature, particularly those related to the identification of key geomorphological parameters, such as the active river channel. These parameters will then serve as fundamental components for carrying out more advanced analyses of geomorphological dynamics.

In the last decades, fluvial researchers have developed methods to characterize the main macro units—water, vegetation, and exposed sediments [9,48,49]—and to investigate changes in river morphology [50], such as vegetation encroachment [51,52] and meander sinuosity and migration rate [39,53]. In most cases, single images were used, with the notable exceptions of [28,32]. The continuous increase in the temporal resolution of satellite data, with weekly and sometimes daily images, allows the use of a temporal reducer to

filter out small-scale variations and identify the different geomorphic macro units more accurately. For many geomorphological applications, the relevant time scale is notably longer than the data acquisition frequency, and the use of an annual or seasonal synthetic image can help to identify the relevant changes.

Furthermore, the proposed approach for multitemporal active channel mapping underpins the inherent dynamicity of riverscapes over space and time, including the spatially explicit relative frequency of the river occupying its erodible corridor. In riverscape monitoring and management, such spatiotemporal metrics represent the necessary shift from single-epoch assessments and metrics to inter-epoch ones. In this perspective, the proposed methodology was found to be capable of delineating the multitemporal active channel at the reach scale and provides a tool for selecting the appropriate temporal resolution, taking into account the processes to be monitored and the associated dynamics of water, sediment, and vegetation. Due to the lack of morphologically-based approaches to define the riverine domain, it is common to approximate the riverscape from global datasets derived from other sources. For example, the Global Surface Water Extent (GSWE) [7] provides the spatial extent of water surfaces over time from 1985 to 2020. With an appropriate buffer, the GSWE represents a valid approximation of the multitemporal active channel from 1985, but it does not account for the presence and dynamics of exposed sediments and in-channel vegetation within the river corridor.

Our work provides a fast and robust delineation of the active channel, using an original procedure based on geomorphologic processes that can be easily adapted to different contexts. After testing the methodology on three different Mediterranean rivers, we can outline some major suggestions (synthesized in Figure 10) for working with cloud computing and medium-resolution multispectral remote sensing data, such as Landsat and Sentinel-2 data, in particular for the delineation of the river active channel:

- The application of temporal reducers is a valid approach to obtain representative synthetic images that can be used to delineate the active channel on an annual or seasonal scale. However, synthetic images computed from single bands or from considered indexes (in this caseNDVI and MNDWI) produce different results, with the former overestimating the active channel compared to the index approach.
- The choice of the percentile of temporal reduction substantially affects the extraction of the active channel. Our work suggests using the 90th percentile with respect to the median.
- An annual temporal resolution is preferable for the computation of the active channel envelope over time in Mediterranean biogeoclimatic regions. Indeed, the annual temporal resolution improves the detection of the riverbed and the distinction from the floodplain in the three case studies. However, the difference between the annual and the seasonal multitemporal active channels is minor. A proper investigation of its effects in other biogeoclimatic regions of the planet is suggested.

Regarding the last point, only an appropriate adaptation of the procedure could enhance ecological and environmental assessments by tailoring remote sensing approaches to specific climatic conditions. This would enable more accurate and contextually meaningful interpretations of vegetation and hydrological dynamics. For instance, Arctic regions present a thermal control not only on vegetation seasonality but also on the hydrological regime. Thus, the seasonal window for vegetation, from May to October [54], is the same as the main hydrological activity [55]. In winter, rivers are at low flow and are mostly frozen, with ice and snow making it difficult to detect riverscape features from multispectral imagery. Improvements in water and ice detection are expected with the use of new hyperspectral data (e.g., PRISMA, IRIDE missions). So far, in the Arctic context, it is reasonable to limit the active channel extraction to the summer months. Similarly, investigations in tropical regions with clearly defined rainy seasons may benefit from different, shorter periods over which the synthetic images and the active channel are derived [56]. In addition, we expect differences when considering rivers where the main riparian species are deciduous or evergreen, as this may produce different temporal patterns of the NDVI index.

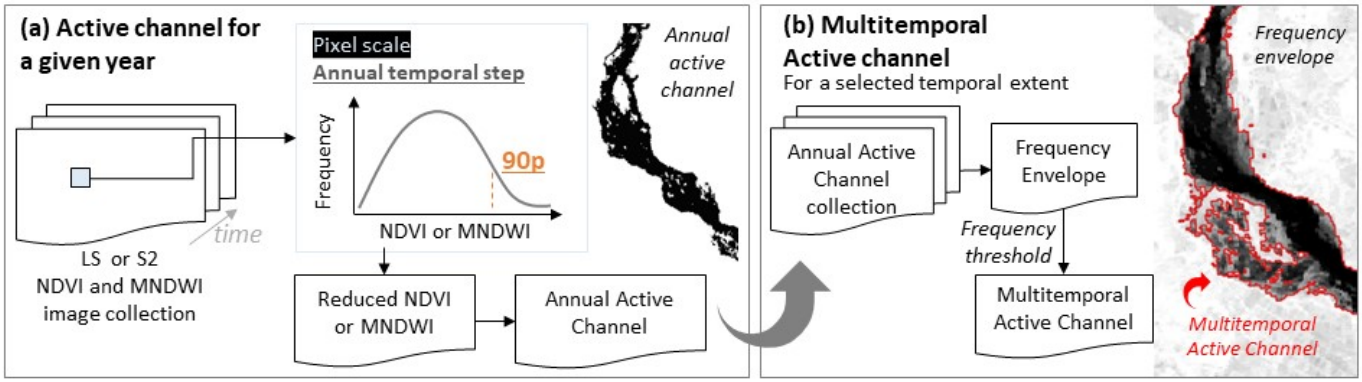

Figure 10. Suggested approach for riverine active channel extraction from Landsat and Sentinel-2 data within GEE.

Once the active channel has been defined, researchers may be interested in observing and monitoring different processes characterized by specific spatiotemporal scales and resolutions, such as channel lateral migration, riparian vegetation recruitment, growth and erosion, or inundation dynamics. Each process should be observed at the appropriate spatiotemporal scale, which may be different from that used to define the riverine domain. For example, intra-seasonal vegetation dynamics can be investigated at weekly or monthly resolution, covering the temporal extent of the vegetative season, with Sentinel-2 or higher-resolution imagery. At an even finer temporal resolution, single images could be used to compute water coverage, coupled with water level or discharge measured on the same day and time of image acquisition [57]. It should be noted that, in this work, the water mask is defined with a fixed threshold of the 90th percentile synthetic MNDWI index, for comparison purposes only. For more detailed wet channel monitoring, more advanced extraction procedures are suggested, such as Canny Edge detection and subsequent buffering to apply an adaptive thresholding approach [58].

According to [59], Google Earth Engine offers rapid and immediate access to understanding a river's capacity for adjustment to changes in environmental conditions, such as water and sediment fluxes. Monitoring this adjustment process, in the case of both natural and anthropogenic changes, provides information about river sensitivity [60]. This includes gaining insight into the range of variability and how different river reaches adapt, along with the reasons for these adjustments. The implementation of models in the GEE platform helps to assess the role of disturbance events and the off-site consequences of river adjustments, thus supporting the interpretation of the evolutionary trajectory of rivers. Clear procedures and a cloud computing environment can also help to further integrate ecological, hydrological, and morphological data and concepts, and foster collaborative research networks that address the study and management of riverscapes as macrosystems [61]. As pointed out by [23], the increasing amount of satellite imagery calls for "big data infrastructure", capable of processing data and producing outputs in an automated way, to inform river managers and enable continuous monitoring [62]. Indeed, one of the major challenges for river scientists remains the transfer of river geomorphology [59] and RS approach [22] to practitioners—as managers and stakeholders—for systematic monitoring as a source for decision-making and well-informed management of riparian zones. The combination of remotely sensed imagery, characterized by increasing spatial, temporal, and spectral resolution, with cloud computing, such as GEE, provides a powerful tool to apply methods and concepts developed in the last decade [63–65] to better understand the recent morphological trajectories of river systems and thus assess their ecosystem potential.

5. Conclusions

The procedure proposed in this work improves our ability to extract—in an accurate and effective manner—the fluvial erodible corridor, which is considered a fundamental step in understanding the morphology and dynamics of a river system [24]. In particular, we

highlight an increased accuracy in the detection of the active channel using synthetic images derived from multispectral indexes (such as NDVI and MDWI) than when using synthetic images derived from single bands. We also quantify the effect of using different percentiles as temporal reducers on a collection of images. For the investigated Mediterranean braided rivers, with dry summer and deciduous vegetation, we suggest the use of the 90p instead of the median to better classify vegetated areas compared to the active water and sediment areas. Taking into account the hydrological and bioclimatic adaptations already discussed, add[]the application of this procedure can be easily extended to many rivers, and is particularly relevant where other topographic data and surveys are missing or fragmented. Moreover, the use of cloud-based computing allows the application at a wide range of spatial scales, from single rivers to whole catchments and regional studies. To this end, the developed and available Python script could be easily converted into a more user-friendly Google Earth Engine online App, accessed 17 October 2023 https://www.earthengine.app/ to further enhance its use by managers and practitioners for river management, conservation and restoration.

Author Contributions: Conceptualization, M.C., A.V. and W.B.; methodology, M.C., A.V. and W.B.; Software, M.C.; Formal analysis, M.C.; writing—original draft preparation, M.C.; writing—review and editing, M.C., A.V., G.Z. and W.B.; supervision, A.V., W.B. and G.Z.; funding acquisition, A.V. and G.Z. All authors have read and agreed to the published version of the manuscript.

Funding: This work was realized in the framework of the activities of the UNESCO Chair in Engineering for Human and Sustainable Development of the University of Trento. Financial support has been provided by VIS (Volontariato Internazionale per lo Sviluppo) and CESVI Onlus within "GREEN coAL-ITion: Eco-sustainable Development for Albanian mountain-countryside natural capital" project [Lot1: CIG 81366342CA]. It has also been supported by the Italian Ministry of Universities and Research (MUR), in the framework of the project DICAM-EXC (Departments of Excellence 2023-2027, grant L232/2016).

Data Availability Statement: The Landsat and Sentinel-2 imagery acquired and associated metadata are available via the Earth Engine's public data archive: https://developers.google.com/earth-engine/datasets/catalog/landsat and https://developers.google.com/earth-engine/datasets/catalog/sentinel, respectively (accessed on 1 January 2022). The code developed for the analysis is publicly available at https://doi.org/10.5281/zenodo.8420993, accessed on 17 October 2023.

Conflicts of Interest: The authors declare no conflicts of interest.

References

1. Smith, L.C. Satellite remote sensing of river inundation area, stage, and discharge: A review. *Hydrol. Process.* **1997**, *11*, 1427–1439. [CrossRef]
2. Alsdorf, D.E.; Lettenmaier, D.P. Tracking Fresh Water from Space. *Science* **2003**, *301*, 1491–1494. [CrossRef] [PubMed]
3. Bizzi, S.; Demarchi, L.; Grabowski, R.C.; Weissteiner, C.J.; de Bund, W.V. The use of remote sensing to characterise hydromorphological properties of European rivers. *Aquat. Sci.* **2016**, *78*, 57–70. [CrossRef]
4. Piégay, H.; Arnaud, F.; Belletti, B.; Bertrand, M.; Bizzi, S.; Carbonneau, P.; Dufour, S.; Liébault, F.; Ruiz-Villanueva, V.; Slater, L. Remotely sensed rivers in the Anthropocene: State of the art and prospects. *Earth Surf. Process. Landf.* **2020**, *45*, 157–188. [CrossRef]
5. Church, M. The trajectory of geomorphology. *Prog. Phys. Geogr. Earth Environ.* **2010**, *34*, 265–286. [CrossRef]
6. Passalacqua, P.; Belmont, P.; Staley, D.M.; Simley, J.D.; Arrowsmith, J.R.; Bode, C.A.; Crosby, C.; DeLong, S.B.; Glenn, N.F.; Kelly, S.A.; et al. Analyzing high resolution topography for advancing the understanding of mass and energy transfer through landscapes: A review. *Earth-Sci. Rev.* **2015**, *148*, 174–193. [CrossRef]
7. Pekel, J.F.; Cottam, A.; Gorelick, N.; Belward, A.S. High-resolution mapping of global surface water and its long-term changes. *Nature* **2016**, *540*, 418–422. [CrossRef]
8. Boothroyd, R.J.; Williams, R.D.; Hoey, T.B.; Barrett, B.; Prasojo, O.A. Applications of Google Earth Engine in fluvial geomorphology for detecting river channel change. *Wiley Interdiscip. Rev. Water* **2021**, *8*, e21496. [CrossRef]
9. Spada, D.; Molinari, P.; Bertoldi, W.; Vitti, A.; Zolezzi, G. Multi-Temporal Image Analysis for Fluvial Morphological Characterization with Application to Albanian Rivers. *ISPRS Int. J. Geo-Inf.* **2018**, *7*, 314. [CrossRef]
10. Feng, D.; Gleason, C.J.; Lin, P.; Yang, X.; Pan, M.; Ishitsuka, Y. Recent changes to Arctic river discharge. *Nat. Commun.* **2021**, *12*, 6917. [CrossRef]

11. Bertoldi, W.; Piégay, H.; Buffin-Bélanger, T.; Graham, D.; Rice, S. Applications of Close-Range Imagery in River Research. In *Fluvial Remote Sensing for Science and Management*; John Wiley & Sons, Ltd.: Chichester, UK, 2012; pp. 341–366. [CrossRef]
12. Belletti, B.; Dufour, S.; Piégay, H. Regional assessment of the multi-decadal changes in braided riverscapes following large floods (Example of 12 reaches in South East of France). *Adv. Geosci.* **2013**, *37*, 57–71. [CrossRef]
13. Nones, M. Remote sensing and GIS techniques to monitor morphological changes along the middle-lower Vistula river, Poland. *Int. J. River Basin Manag.* **2021**, *19*, 345–357. [CrossRef]
14. Boothroyd, R.J.; Williams, R.D.; Hoey, T.B.; Tolentino, P.L.; Yang, X. National-scale assessment of decadal river migration at critical bridge infrastructure in the Philippines. *Sci. Total Environ.* **2021**, *768*, 144460. [CrossRef] [PubMed]
15. Demarchi, L.; Bizzi, S.; Piégay, H. Regional hydromorphological characterization with continuous and automated remote sensing analysis based on VHR imagery and low-resolution LiDAR data. *Earth Surf. Process. Landf.* **2017**, *42*, 531–551. [CrossRef]
16. Bizzi, S.; Piégay, H.; Demarchi, L.; de Bund, W.V.; Weissteiner, C.; Gob, F. LiDAR-based fluvial remote sensing to assess 50–100-year human-driven channel changes at a regional level: The case of the Piedmont Region, Italy. *Earth Surf. Process. Landf.* **2019**, *44*, 471–489. [CrossRef]
17. Cavallo, C.; Nones, M.; Papa, M.N.; Gargiulo, M.; Ruello, G. Monitoring the morphological evolution of a reach of the Italian Po River using multispectral satellite imagery and stage data. *Geocarto Int.* **2022**, *37*, 8579–8601. [CrossRef]
18. Gorelick, N.; Hancher, M.; Dixon, M.; Ilyushchenko, S.; Thau, D.; Moore, R. Google Earth Engine: Planetary-scale geospatial analysis for everyone. *Remote Sens. Environ.* **2017**, *202*, 18–27. [CrossRef]
19. Tobón-Marín, A.; Barriga, J.C. Analysis of changes in rivers planforms using Google Earth Engine. *Int. J. Remote Sens.* **2020**, *41*, 8654–8681. [CrossRef]
20. Vercruysse, K.; Grabowski, R.C. Human impact on river planform within the context of multi-timescale river channel dynamics in a Himalayan river system. *Geomorphology* **2021**, *381*, 107659. [CrossRef]
21. Pavelsky, T.M.; Smith, L.C. RivWidth: A Software Tool for the Calculation of River Widths From Remotely Sensed Imagery. *IEEE Geosci. Remote Sens. Lett.* **2008**, *5*, 70–73. [CrossRef]
22. Rusnák, M.; Goga, T.; Michaleje, L.; Šulc Michalková, M.; Máčka, Z.; Bertalan, L.; Kidová, A. Remote Sensing of Riparian Ecosystems. *Remote Sens.* **2022**, *14*, 2645. [CrossRef]
23. Tomsett, C.; Leyland, J. Remote sensing of river corridors: A review of current trends and future directions. *River Res. Appl.* **2019**, *35*, 779–803. [CrossRef]
24. Piégay, H.; Darby, S.E.; Mosselman, E.; Surian, N. A review of techniques available for delimiting the erodible river corridor: A sustainable approach to managing bank erosion. *River Res. Appl.* **2005**, *21*, 773–789. [CrossRef]
25. Ashmore, P. *9.17 Morphology and Dynamics of Braided Rivers*; Elsevier: Amsterdam, The Netherlands, 2013; pp. 289–312. [CrossRef]
26. Belletti, B.; Rinaldi, M.; Bussettini, M.; Comiti, F.; Gurnell, A.M.; Mao, L.; Nardi, L.; Vezza, P. Characterising physical habitats and fluvial hydromorphology: A new system for the survey and classification of river geomorphic units. *Geomorphology* **2017**, *283*, 143–157. [CrossRef]
27. Diniz, C.; Cortinhas, L.; Nerino, G.; Rodrigues, J.; Sadeck, L.; Adami, M.; Souza-Filho, P. Brazilian Mangrove Status: Three Decades of Satellite Data Analysis. *Remote Sens.* **2019**, *11*, 808. [CrossRef]
28. Boothroyd, R.J.; Nones, M.; Guerrero, M. Deriving Planform Morphology and Vegetation Coverage From Remote Sensing to Support River Management Applications. *Front. Environ. Sci.* **2021**, *9*, 657354. [CrossRef]
29. Foga, S.; Scaramuzza, P.L.; Guo, S.; Zhu, Z.; Dilley, R.D.; Beckmann, T.; Schmidt, G.L.; Dwyer, J.L.; Joseph Hughes, M.; Laue, B. Cloud detection algorithm comparison and validation for operational Landsat data products. *Remote Sens. Environ.* **2017**, *194*, 379–390. [CrossRef]
30. Rouse, J.W.; Haas, R.H.; Schell, J.A.; Deering, D.W. Monitoring vegetation systems in the Great Plains with ERTS. *NASA Spec. Publ.* **1974**, *351*, 309.
31. Xu, H. Modification of normalised difference water index (NDWI) to enhance open water features in remotely sensed imagery. *Int. J. Remote Sens.* **2006**, *27*, 3025–3033. [CrossRef]
32. Yadav, A.; Boothroyd, R.J.; Smith, G.H.S.; Sen, S. Morphological adjustments of the Yamuna River in the Himalayan foothills in response to natural and anthropogenic stresses. *Hydrol. Process.* **2023**, *37*, e14934. [CrossRef]
33. ASIG 2015 Orthophoto. Available online: https://geoportal.asig.gov.al/geonetwork/srv/eng/catalog.search#/metadata/b50abc17-b932-4a96-b97a-ae6cba52c2fb (accessed on 1 July 2023).
34. Tockner, K.; Ward, J.V.; Arscott, D.B.; Edwards, P.J.; Kollmann, J.; Gurnell, A.M.; Petts, G.E.; Maiolini, B. The Tagliamento River: A model ecosystem of European importance. *Aquat. Sci. Res. Across Bound.* **2003**, *65*, 239–253. [CrossRef]
35. Schiemer, F.; Beqiraj, S.; Drescher, A.; Graf, W.; Egger, G.; Essl, F.; Frank, T.; Hauer, C.; Hohensinner, S.; Miho, A.; et al. The Vjosa River corridor: A model of natural hydro-morphodynamics and a hotspot of highly threatened ecosystems of European significance. *Landsc. Ecol.* **2020**, *35*, 953–968. [CrossRef]
36. Bajrami, F.; Crivellaro, M.; Cekrezi, B.; Skrame, K.; Zolezzi, G. The Shkumbin River, Albania: hydromorphological evolution phases. In Proceedings of the 5th International Conference on "The Status and Future of the World's Large Rivers", Vienna, Austria, 21–25 August 2023.
37. Gurnell, A.M.; Bertoldi, W.; Corenblit, D. Changing river channels: The roles of hydrological processes, plants and pioneer fluvial landforms in humid temperate, mixed load, gravel bed rivers. *Earth-Sci. Rev.* **2012**, *111*, 129–141. [CrossRef]

38. Crivellaro, M.; Serrao, L.; Bertoldi, W.; Bizzi, S.; Vitti, A.; Zolezzi, G. Morphological response to climatic and anthropic pressures of the Vjosa river, a reference system for river management and restoration. In Proceedings of the EGU General Assembly Conference Abstracts, Vienna, Austria, 3–8 April 2022; p. EGU22–9135.
39. Monegaglia, F.; Zolezzi, G.; Güneralp, I.; Henshaw, A.J.; Tubino, M. Automated extraction of meandering river morphodynamics from multitemporal remotely sensed data. *Environ. Model. Softw.* **2018**, *105*, 171–186. [CrossRef]
40. True Ortofoto della Regione Friuli Venezia Giulia, 2017–2020. Available online: https://www.regione.fvg.it/rafvg/cms/RAFVG/ambiente-territorio/conoscere-ambiente-territorio/FOGLIA5/ (accessed on 1 July 2023).
41. Rinaldi, M.; Surian, N.; Comiti, F.; Bussettini, M. A methodological framework for hydromorphological assessment, analysis and monitoring (IDRAIM) aimed at promoting integrated river management. *Geomorphology* **2015**, *251*, 122–136. [CrossRef]
42. Pano, N. Dinamica del litorale albanese (sintesi delle conoscenze). In *Atti del 10° Congresso della Associazione Italiana di Oceanologia e Limnologia*; G. Lang Publishers: Genova, Italy, 1992; pp. 3–18.
43. Ciavola, P. Relation between river dynamics and coastal changes in Albania: An assessment integrating satellite imagery with historical data. *Int. J. Remote Sens.* **1999**, *20*, 561–584. [CrossRef]
44. Bertoldi, W.; Gurnell, A.; Surian, N.; Tockner, K.; Zanoni, L.; Ziliani, L.; Zolezzi, G. Understanding reference processes: Linkages between river flows, sediment dynamics and vegetated landforms along the Tagliamento River, Italy. *River Res. Appl.* **2009**, *25*, 501–516. [CrossRef]
45. Nanson, G.; Croke, J. A genetic classification of floodplains. *Geomorphology* **1992**, *4*, 459–486. [CrossRef]
46. Zhai, K.; Wu, X.; Qin, Y.; Du, P. Comparison of surface water extraction performances of different classic water indices using OLI and TM imageries in different situations. *Geo-Spat. Inf. Sci.* **2015**, *18*, 32–42. [CrossRef]
47. Bertoldi, W.; Drake, N.A.; Gurnell, A.M. Interactions between river flows and colonizing vegetation on a braided river: Exploring spatial and temporal dynamics in riparian vegetation cover using satellite data. *Earth Surf. Process. Landf.* **2011**, *36*, 1474–1486. [CrossRef]
48. Henshaw, A.J.; Gurnell, A.M.; Bertoldi, W.; Drake, N.A. An assessment of the degree to which Landsat TM data can support the assessment of fluvial dynamics, as revealed by changes in vegetation extent and channel position, along a large river. *Geomorphology* **2013**, *202*, 74–85. [CrossRef]
49. Carbonneau, P.E.; Belletti, B.; Micotti, M.; Lastoria, B.; Casaioli, M.; Mariani, S.; Marchetti, G.; Bizzi, S. UAV-based training for fully fuzzy classification of Sentinel-2 fluvial scenes. *Earth Surf. Process. Landf.* **2020**, *45*, 3120–3140. [CrossRef]
50. Demarchi, L.; Bizzi, S.; Piégay, H. Hierarchical Object-Based Mapping of Riverscape Units and in-Stream Mesohabitats Using LiDAR and VHR Imagery. *Remote Sens.* **2016**, *8*, 97. [CrossRef]
51. Hervouet, A.; Dunford, R.; Piégay, H.; Belletti, B.; Trémélo, M.L. Analysis of post-flood recruitment patterns in braided-channel rivers at multiple scales based on an image series collected by unmanned aerial vehicles, ultra-light aerial vehicles, and satellites. *GISci. Remote Sens.* **2011**, *48*, 50–73. [CrossRef]
52. Latella, M.; Bertagni, M.B.; Vezza, P.; Camporeale, C. An Integrated Methodology to Study Riparian Vegetation Dynamics: From Field Data to Impact Modeling. *J. Adv. Model. Earth Syst.* **2020**, *12*, e2020MS002094. [CrossRef] [PubMed]
53. Yousefi, S.; Pourghasemi, H.R.; Hooke, J.; Navratil, O.; Kidová, A. Changes in morphometric meander parameters identified on the Karoon River, Iran, using remote sensing data. *Geomorphology* **2016**, *271*, 55–64. [CrossRef]
54. Ernakovich, J.G.; Hopping, K.A.; Berdanier, A.B.; Simpson, R.T.; Kachergis, E.J.; Steltzer, H.; Wallenstein, M.D. Predicted responses of arctic and alpine ecosystems to altered seasonality under climate change. *Glob. Chang. Biol.* **2014**, *20*, 3256–3269. [CrossRef]
55. Bring, A.; Fedorova, I.; Dibike, Y.; Hinzman, L.; Mård, J.; Mernild, S.H.; Prowse, T.; Semenova, O.; Stuefer, S.L.; Woo, M. Arctic terrestrial hydrology: A synthesis of processes, regional effects, and research challenges. *J. Geophys. Res. Biogeosci.* **2016**, *121*, 621–649. [CrossRef]
56. Serrao, L.; Brentari, L.; Terrones, L.E.B.; Yupanqui, H.A.H.; Trigoso, J.P.R.; Zolezzi, G. Hydro-Morphological Disturbance and Suitability for Temporary Agriculture of Riverine Islands in a Tropical Wandering River. *Water Resour. Res.* **2022**, *58*, e2021WR030674. [CrossRef]
57. Rossi, D.; Zolezzi, G.; Bertoldi, W.; Vitti, A. Monitoring Braided River-Bed Dynamics at the Sub-Event Time Scale Using Time Series of Sentinel-1 SAR Imagery. *Remote Sens.* **2023**, *15*, 3622. [CrossRef]
58. Donchyts, G.; Schellekens, J.; Winsemius, H.; Eisemann, E.; van de Giesen, N. A 30 m Resolution Surface Water Mask Including Estimation of Positional and Thematic Differences Using Landsat 8, SRTM and OpenStreetMap: A Case Study in the Murray-Darling Basin, Australia. *Remote Sens.* **2016**, *8*, 386. [CrossRef]
59. Brierley, G.; Fryirs, K. Truths of the Riverscape: Moving beyond command-and-control to geomorphologically informed nature-based river management. *Geosci. Lett.* **2022**, *9*, 14. [CrossRef]
60. Fryirs, K.A. River sensitivity: A lost foundation concept in fluvial geomorphology. *Earth Surf. Process. Landf.* **2017**, *42*, 55–70. [CrossRef]
61. Gurnell, A.M.; Bertoldi, W.; Tockner, K.; Wharton, G.; Zolezzi, G. How large is a river? Conceptualizing river landscape signatures and envelopes in four dimensions. *WIREs Water* **2016**, *3*, 313–325. [CrossRef]
62. de Moraes Frasson, R.P.; Pavelsky, T.M.; Fonstad, M.A.; Durand, M.T.; Allen, G.H.; Schumann, G.; Lion, C.; Beighley, R.E.; Yang, X. Global Relationships Between River Width, Slope, Catchment Area, Meander Wavelength, Sinuosity, and Discharge. *Geophys. Res. Lett.* **2019**, *46*, 3252–3262. [CrossRef]

63. Gurnell, A.M.; Rinaldi, M.; Belletti, B.; Bizzi, S.; Blamauer, B.; Braca, G.; Buijse, A.D.; Bussettini, M.; Camenen, B.; Comiti, F.; et al. A multi-scale hierarchical framework for developing understanding of river behaviour to support river management. *Aquat. Sci.* **2016**, *78*, 1–16. [CrossRef]
64. Rinaldi, M.; Gurnell, A.M.; del Tánago, M.G.; Bussettini, M.; Hendriks, D. Classification of river morphology and hydrology to support management and restoration. *Aquat. Sci.* **2016**, *78*, 17–33. [CrossRef]
65. Grabowski, R.C.; Surian, N.; Gurnell, A.M. Characterizing geomorphological change to support sustainable river restoration and management. *Wiley Interdiscip. Rev. Water* **2014**, *1*, 483–512. [CrossRef]